

## Hybrid Simulation of the Surface Mounted Square Cylinder

J. Weatheritt and R. D. Sandberg

Department of Mechanical Engineering  
University of Melbourne, Victoria 3010, Australia

### Abstract

The simulation of a finite surface mounted square cylinder placed in a turbulent boundary layer is presented. We use a newly developed hybrid RANS/LES approach in order to validate it for a fully three dimensional flow and highlight the efficacy of the numerical aspects of the methodology. Agreement is excellent with reference DNS, for both mean statistics and spectral content. The mean field is scrutinised, particularly the free end flow, which shows qualitatively different features from those typically seen over the free end of a surface mounted circular cylinder.

### Introduction

Flows around finite bluff bodies obstructing attached boundary layers are prevalent in practical engineering problems. Particularly, during the design of high-rise buildings, pedestrian comfort at ground level must be considered. For extremely tall buildings, the complex vortex shedding must be understood to guarantee structural integrity. Often the Reynolds number exceeds those practical for direct numerical simulation (DNS) and even large eddy simulation (LES) where as Reynolds-averaged techniques (RANS) are often too inaccurate for the prediction of three dimensional and separated flows. Therefore methods that compromise between these approaches offer a promising alternative.

The flow around such a body, mounted in a developed shear flow is characterised by several features. Firstly, the oncoming boundary layer separates due to the adverse pressure gradient induced by the body. This forms a series of horseshoe or neck-lace vortices that wrap around the structure [1]. At the mounting point, a series of streamwise coherent structures are shed, which have become known as base vortices [11]. At the free end, depending on the ratios of height to diameter  $h/d$  and boundary layer thickness  $h/\delta$  each a function of Reynolds number  $Re$ , the flow may separate at the leading edge or separate in two counter rotating spiral vortices beyond the leading edge [8]. This separated shear layer, often recognised as a pair of tip vortices, is then convected downstream and induces a downwash that acts to modulate the separated flow.

Perhaps independently, another critical value of the above ratios allows for two flow regimes in the near wake. Above the critical value, the flow around the sides of the body is able to shed in a von-Kármán street, like that present behind infinite cylinders, but the up- and downwashes from the base and tip vortices act to shift the phase angle which produces a lag in the vortex street formation. Below this, Wang and Zhou [11] attributes the suppression of this shedding as a consequence of the dominant symmetric upwash and downwash regimes. The flow pattern is then described as an arch-type vortex which has been visualised experimentally many body diameters downstream [5].

In this study we perform a hybrid RANS/LES of a square mounted cylinder in the configuration of recent numerical [10] and experimental studies [2]. The purpose of this study is twofold. Firstly, the case serves to validate our hybrid RANS/LES method [12, 13] for a fully three-dimensional flow

field. In reporting this, we also display the efficacy of the numerical framework. Secondly, once validated we probe the resulting database for information regarding the vortical structures embedded in the flow field.

### Flow Configuration and Numerical Methodology

The Reynolds number based on diameter  $d$  and freestream velocity  $U_\infty$  is  $Re=11,000$ . The incoming zero pressure gradient boundary layer has a momentum thickness Reynolds number  $Re_\theta = 790$  at  $x/d = -8$  and relative to the cylinder diameter has a height  $\delta/d = 0.72$ . The square cylinder is of aspect ratio  $h/d = 4$ , with its base at the origin. The plate is placed in the  $x-y$  plane at  $z = 0$ . The full simulation domain is  $-8 \leq x/d \leq 16$ ,  $|y/d| \leq 8$  and  $0 \leq z \leq 12$ . The total mesh count was 20 million cells, with  $x^+$ ,  $y^+$  and  $z^+ < 1$ . This is a relatively fine mesh for hybrid RAN/LES; the reference DNS used 250 million cells. However, fine mesh hybrid simulations are not without their challenges, as discussed below and using a hybrid gives us the luxury of not requiring fluctuations in the incoming boundary layer. By solving this region as RANS, a method well calibrated for this flow regime, we gain confidence in our attached boundary layer. Note that the nature of the geometry makes this an inherently expensive simulation and a saving factor of 12.5 over the DNS is not insignificant. Statistics were gathered for  $1500d/U_\infty$  time units, which equates to 170 shedding cycles.

The hybrid methodology [12, 13] spatially and temporally damps the turbulent length scale  $\ell_t$  in the RANS model of Speziale, Sarkar and Gatski [7],

$$\ell^{hyb} = f\ell_t. \quad (1)$$

The damping function  $f$  should vary between 0 and 1. The former switching off the model on very fine meshes and the latter fully activating the turbulence model to operate in full RANS mode. The function,

$$f = \min \left[ \frac{\overbrace{\min \left( c_1 \frac{\Delta}{\ell_t}, 1 \right)}^{\text{DES style}} \overbrace{\min \left( \log \left( 1 + c_2 \frac{\Delta}{\ell_\eta} \right)^{c_3}, 1 \right)}^{\text{effective coefficient}}}{\underbrace{1 - f_b + 1^{-20}}_{\text{shield}}}, 1 \right] \quad (2)$$

is the result of an evolutionary algorithm [12]. The resulting function was found to be similar to Detached-Eddy Simulation (DES) [6], but with an extra effective coefficient term that lowers the coefficient  $c_1$  in the DNS limit. The ‘shield’ term has been adopted from previous work [14] and is responsible for enforcing a RANS solution near the wall.  $f_b$  is a damping function from the SST [4] turbulence model,  $\ell_\eta$  is the Kolmogorov length scale,  $\Delta = \max(\Delta_x, \Delta_y, \Delta_z)$  is the grid length scale and  $c_1 = 2.1$ ,  $c_2 = 0.75$  and  $c_3 = 4$  are calibrated model coefficients. To complement the physical model, the numerics must blend from a dissipative scheme in the RANS regime, to a more accurate scheme when resolving turbulence. The purpose of this is twofold: the dissipation in the RANS zone can enforce the

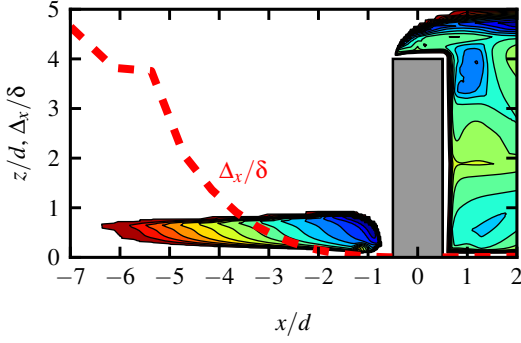


Figure 1: Time averaged  $f$  in the centre plane. White is RANS mode ( $f = 1$ ), the contours reduce from red (0.99) to blue (0) in 11 intervals. (---)  $\Delta_x/\delta$ .

model to stay in RANS mode and lowering the dissipation of the numerical scheme can assist the transition to LES. Therefore the numerical scheme must be a function of  $f$ . We use a blending between upwinding and central differencing,

$$\sigma^{\text{hyb}} = \psi \sigma^{\text{up}} + (1 - \psi) \sigma^{\text{cds}}, \quad (3)$$

via the use of a function  $\psi = \psi(f)$ . This provides a direct mapping between model contribution level  $f$  and required scheme blending  $\sigma^{\text{hyb}}$  that is bound for realizable values of  $f$ . In this work  $\psi$  is defined as,

$$\psi = \min \left[ 1, \frac{1}{1 - g + 10^{-20}} \max \left( 1 - \exp^{-s_2 f^{s_3}}, s_1 \right) \right]. \quad (4)$$

For upwinding in RANS regions, stabilising upwinding for  $0.4 < f < 0.6$  and central differencing for  $f < 0.4$ , the constants are set to  $s_1 = 0$ ,  $s_2 = 12$  and  $s_3 = 10$ .

The function  $g$  is prepended in Eq. 4, in a fashion similar to Travin *et al.* [9], which ensures the LES mode only becomes active in regions of strong vortical flow. We define  $g$  as

$$g = \frac{1}{2} - \frac{1}{2} \frac{\Omega^2 - S^2}{\Omega^2 + S^2}, \quad (5)$$

where  $S$  and  $\Omega$  are the magnitudes of the strain and rotation rate tensors.

For hybrid methodologies, a phenomenon known as model stress depletion [6] can affect the prediction in attached bound-

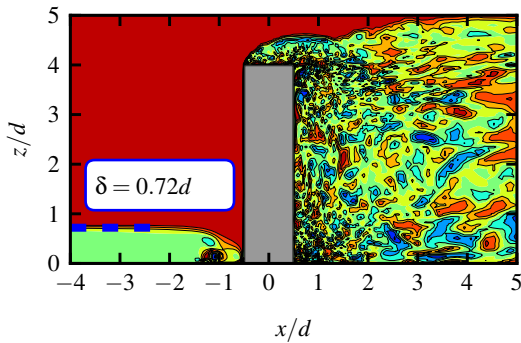


Figure 2: Contours of  $g$ . Ten evenly spaced levels from 0 (blue) to 1 (red). For the incoming boundary layer  $g = 0.5$ . (---)  $z/d = \delta/d = 0.72$  highlights the correct detection of the boundary layer edge.

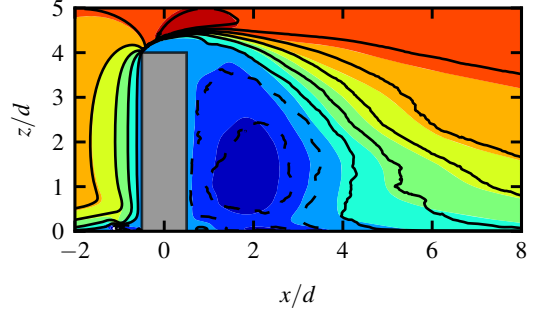


Figure 3: Time averaged streamwise velocity contours  $U/U_\infty$ , levels from -0.5 to 1.3. (—) DNS [10]  $U > 0$ , (---) DNS  $U < 0$ . Fill: hybrid.

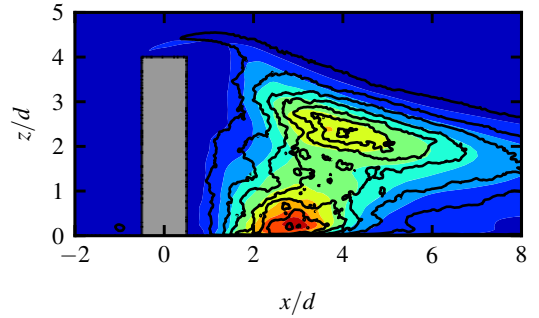


Figure 4: Time averaged Reynolds-stress  $\tau_{yy}$ , levels from 0 to 0.28. (—) DNS [10]. Fill: hybrid.

ary layers. When  $\Delta/\delta < 10$ , the model starts to switch off because it detects high resolution. However, the incoming boundary layer is often desired to be solved as a RANS. For two dimensional problems this can be alleviated by setting  $\Delta_y > 10\delta$ , however for this three dimensional case the spanwise direction is also very well resolved. Figure 1 is a plot of time averaged  $f$ , which clearly shows that as  $\Delta/\delta \ll 10$ , the incoming boundary layer is preserved. This is because  $g$  (shown in Fig. 2) detects strain and holds the boundary layer ( $\delta \approx 0.72d$ ) in RANS mode. Initial studies on this problem with our previous numerical blending [13] show an almost instant relaminarisation at the inflow. Note the strong reduction in  $f$  for  $x/d > -5$  is due to a sharp increase in the pressure gradient and the required resolution of formed horseshoe vortices. Behind the cylinder, in the wake, we can see vortical motions being detected. This ‘allows’ the damping function to lower the model contribution. Indeed, in the base and tip vortices, the average value is  $f < 0.1$ .

## Results

### Validation

To validate our simulation, the original DNS [10] is compared against in Figs. 3-5. These plots show excellent agreement for mean first (streamwise velocity  $U$ ) and second (Reynolds stress  $\tau_{yy}$ ) order statistics and spectral content (Streamwise power spectra  $E_{ii}$ ). Globally, both the incoming adverse pressure gradient boundary layer and recirculation zone have been correctly predicted. The spanwise Reynolds stress shows the correct peaks from the up- and downwash flow and the correct tipping of the profile at the free end. Also, particularly pleasing is the exceptional prediction of the streamwise velocity power spectrum at  $(7d, 3d, 4.2d)$ . Only for  $\phi > 0.8$ , which corresponds to time scales on the order of  $0.4\Delta_x/U$ , does the frequency content differ from DNS. This deviation is expected because the high

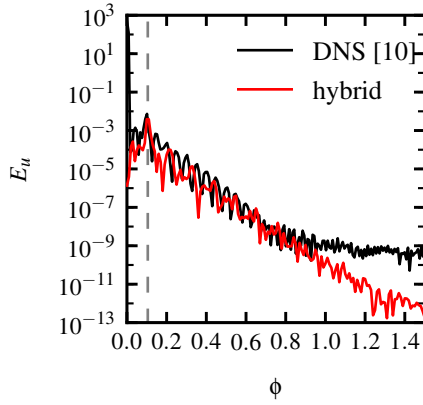


Figure 5: Streamwise velocity power spectral density recorded at  $(7d, 3d, 4.2d)$  against normalised frequency  $\phi$ . (---) shedding frequency.

frequency information is lost when using a coarser resolution.

### Mean Flow Structures

The wall shear stress vector can be used to infer the limiting behaviour of vortices in the vicinity of solid surfaces. This is revealed by considering that the velocity vector is parallel to its gradient in the limit of the wall. Further, it is easily shown that the vorticity vector is orthogonal to all points.

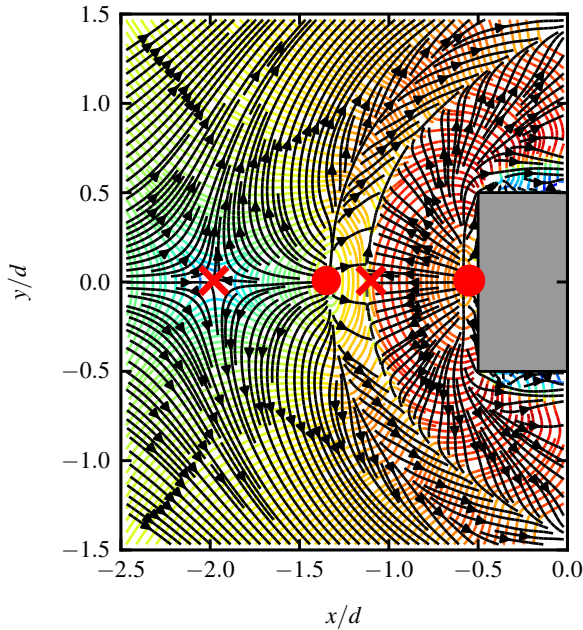


Figure 6: ( $\rightarrow$ ) wall shear stress lines at  $z=0$ . ( $\rightarrow$ ) vorticity lines coloured by magnitude. Red: high values. Blue: low magnitude. (●) reattachment point. (×) saddle point.

Figure 6 is a plot of the time averaged wall shear stress lines and vorticity vector coloured by its magnitude. The separation and reattachment points mark the average footprint of the four counter rotating horseshoe vortices. On the line of symmetry, the saddle points denote separation. The behaviour of the square cylinder matches that of a circular cylinder [1]; that is we see the rollers rotating upwards and towards the body narrower in extent and the primary vortex situated between the third and fourth markers.

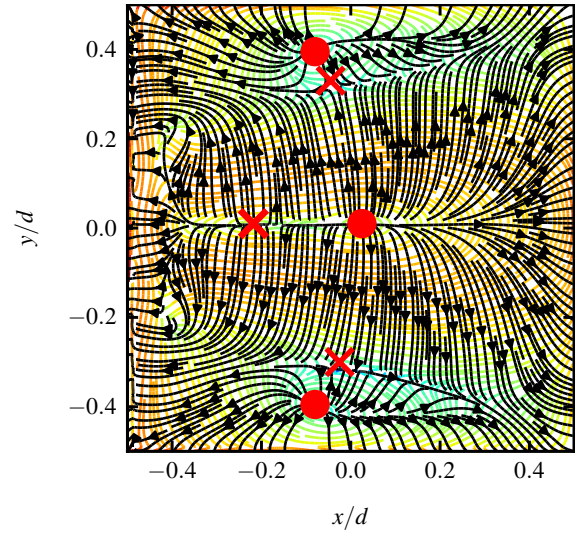


Figure 7: ( $\rightarrow$ ) wall shear stress lines on the free end. ( $\rightarrow$ ) vorticity lines coloured by magnitude. Red: high values. Blue: low magnitude. (●) reattachment point. (×) saddle point.

However, Fig. 7, a similar plot over the free end, shows qualitatively different features from a circular cylinder. As the flow hits the leading edge, it separates and reattaches at the marked circles. From these circles one can follow connecting streamlines around the saddle points. The flow in the centre has formed *two* pairs of  $x$  aligned vortices. One pair is travelling upstream to the leading edge and eventually gets pushed up into the separated shear layer by the upwash flow. The second pair exists behind the line of reattachment and travels towards the trailing edge. Note the saddle point on the line of symmetry is a consequence of the strong pressure gradient near the leading edge; which twists the backward travelling vortices such that, although their footprint travels downstream, their overall direction is upstream. One can also see a third pair of counter rotating vortices, of much weaker angular velocity, sitting outside the central core. These are convected towards the outer corners on the trailing edge. This behaviour has been confirmed via analysis of the full three-dimensional streamlines (not shown).

In comparison, the free end of a cylinder that has undergone bluff body separation (for example see Fig. 6(b) of Krajnovic [3]) does not generate streamwise aligned vortices. In the case of the cylinder, the vorticity vectors remain aligned in the  $y$  direction (unlike the  $x$  presented here). This discrepancy will be due to the combination of separation angle induced by the leading edge topology, boundary layer thickness and aspect ratio of the body.

### Spatial Correlation

The spatial correlation function  $R_w$  about the point  $(2d, 0, 0.5d)$  is displayed on the plane  $y=0$  in Fig. 8 and on the plane  $z/d=0.5$  in Fig. 9. Unsurprisingly, there is strong correlation along the line  $z/d=1$  and a positive/negative pattern indicative of the vortex shedding is observed as we travel downstream. Wall parallel flapping motion can be seen to spread dramatically downstream and the tipping effect of the downwash flow is observed.

### Conclusions

Numerical aspects of a hybrid RANS/LES methodology have been presented for the case of a surface mounted square cylinder. Even in this extreme case, the function  $g$  effectively de-

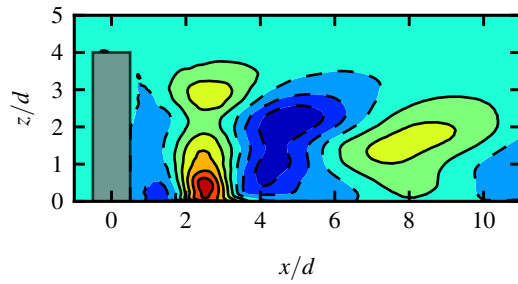


Figure 8: Spatial correlation  $R_{vv}$  with the point  $(2d, 0, 0.5d)$  in the plane  $y = 0$ . Contours are ten evenly spaced levels on the range  $(-0.65, 1)$ . (—) positive value. (- - -) negative value.

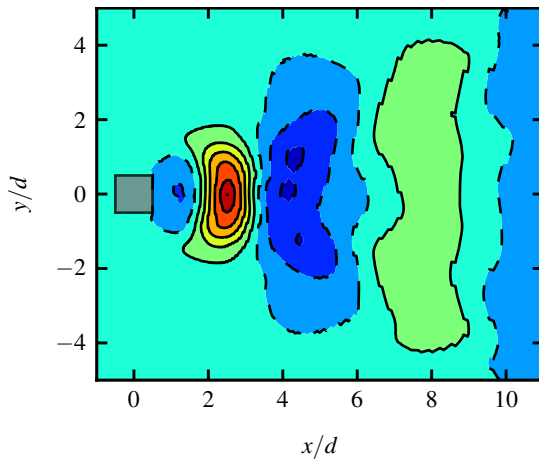


Figure 9: Spatial correlation  $R_{vv}$  with the point  $(2d, 0, 0.5d)$  in the  $z/d = 0.5$ . Contours as in Fig. 8.

tected the edge of the RANS boundary layer as  $\Delta \ll 10\delta$ . The simulation has been validated against highly resolved DNS and shown to match exceptionally well for a range of statistics.

Mean flow lines over the flat plate and free end were presented. Whilst the observed flow pattern on the plate was qualitatively similar to that around a cylinder, the flow over the free end showed streamwise aligned vortices travelling up- and downstream, which is a contrast to that often seen in cylinder experiments. Spatial correlation has revealed the characteristic tip in the vortex shedding process. Time series are now being gathered, with which to adequately analyse the coherency and phase in the vortex shedding. This can then be compared to similar flow problems, in particular the experiments of Wang and Zhou [11].

#### Acknowledgements

We acknowledge the funding from a veski fellowship. This work was also supported by resources provided by The Pawsey Supercomputing Centre with funding from the Australian Government and the Government of Western Australia. A very big thank you to Ricardo Vinuesa and the KTH group, who made their data readily available.

#### References

- [1] Baker, C., The turbulent horseshoe vortex, *Journal of Wind Engineering and Industrial Aerodynamics*, **6**, 1980, 9–23.
- [2] Bourgeois, J., Sattari, P. and Martinuzzi, R. J., Coherent

vortical and straining structures in the finite wall-mounted square cylinder wake, *International Journal of Heat and Fluid Flow*, **35**, 2012, 130–140.

- [3] Krajnović, S., Flow around a tall finite cylinder explored by large eddy simulation, *Journal of Fluid Mechanics*, **676**, 2011, 294–317.
- [4] Menter, F. R., Two-Equation Eddy-Viscosity Turbulence Models for Engineering Applications, *AIAA Journal*, **32**, 1994, 1598–1605.
- [5] Sakamoto, H. and Arie, M., Vortex shedding from a rectangular prism and a circular cylinder placed vertically in a turbulent boundary layer, *J. Fluid Mech*, **126**, 1983, 147–165.
- [6] Spalart, P. R., Deck, S., Shur, M., Squires, K., Strelets, M. K. and Travin, A., A new version of detached-eddy simulation, resistant to ambiguous grid densities, *Theoretical and Computational Fluid Dynamics*, **20**, 2006, 181–195.
- [7] Speziale, C. G., Sarkar, S. and Gatski, T. B., Modelling the pressure-strain correlation of turbulence: an invariant dynamical systems approach, *Journal of Fluid Mechanics*, **227**, 1991, 245–272.
- [8] Sumner, D., Flow above the free end of a surface-mounted finite-height circular cylinder: a review, *Journal of Fluids and Structures*, **43**, 2013, 41–63.
- [9] Travin, A., Shur, M., Strelets, M. and Spalart, P., Physical and numerical upgrades in the detached-eddy simulation of complex turbulent flows, in *Advances in LES of complex flows*, Springer, 2002, 239–254.
- [10] Vinuesa, R., Schlatter, P., Malm, J., Mavriplis, C. and Henningson, D. S., Direct numerical simulation of the flow around a wall-mounted square cylinder under various inflow conditions, *Journal of Turbulence*, **16**, 2015, 555–587.
- [11] Wang, H. and Zhou, Y., The finite-length square cylinder near wake, *Journal of Fluid Mechanics*, **638**, 2009, 453–490.
- [12] Weatheritt, J. and Sandberg, R. D., Hybrid rans/les from symbolic regression: formulation and application, *AIAA Journal — under review*.
- [13] Weatheritt, J., Sandberg, R. D. and Lozano-Durán, A., Reynolds stress structures in the hybrid rans/les of a planar channel, *Journal of Physics: Conference Series*, **708**, 2016, 012008.
- [14] Weinmann, M., Sandberg, R. D. and Doolan, C., Tandem cylinder flow and noise predictions using a Hybrid RANS/LES approach, *International Journal of Heat and Fluid Flow*, **50**, 2014, 263—278.